AIAA Aviation
22-26 June 2015, Dallas, TX
22nd AIAA Computational Fluid Dynamics Conference

Delayed Detached–Eddy Simulation of Shock Buffet on Half Wing–Body Configuration

F. Sartor* and S. Timme†

University of Liverpool, Liverpool, England L69 3GH, United Kingdom

This paper presents a numerical study of the transonic flow over a half wing-body configuration representative of a large civil aircraft. The Mach number is close to cruise conditions, while the high angle of attack causes massive separation on the suction side of the wing. Results indicate the presence of shock-wave oscillations inducing unsteady loads which can cause serious damage to the aircraft. Transonic shock buffet is found. Based on preliminary simulations using a baseline grid, the region relevant to the phenomenon is identified and mesh adaptation is applied to significantly refine the grid locally. Then, time-accurate Reynolds-averaged Navier-Stokes and delayed detached-eddy simulations are performed on the adapted grid. Both types of simulation reproduce the unsteady flow physics and much information can be extracted from the results when investigating frequency content, the location of unsteadiness and its amplitude. Differences and similarities in the computational results are discussed in detail and also analysed with respect to recent experimental data.

I. Introduction

At cruise condition, the flow around the wing of a typical large civil aircraft is characterised by the presence of strong shock waves interacting with the boundary layer to cause massive separation. The consequence is the occurrence of large-scale unsteadiness including significant shock movements, known as shock buffet, which arise for combinations of Mach number and angle of attack.[1] This phenomenon presents an industrial interest and has thus been the subject of numerous studies in the past.

Shock buffet is a phenomenon that can be observed both in two- and three-dimensional configurations, from simple aerofoils to swept wings. In the particular two-dimensional case, the unsteadiness is characterised by harmonic shock motions. There is a large amount of literature discussing experimental investigations,[2,3,4] numerical studies based on unsteady Reynolds-averaged Navier-Stokes (URANS) simulations,[5,6,7] and stability analysis.[8,9,10] More recently, high-fidelity approaches based on hybrid methods such as zonal detached-eddy simulation (ZDES),[11] delayed detached-eddy simulation (DDES)[12] or improved delayed detached-eddy simulation[13] have successfully been applied to two-dimensional profiles.

When considering more challenging configurations, such as a wing representative of a large civil aircraft, the literature is more limited. Experimental investigations have shown the complexity of the shock motions[14] and were able to demonstrate the potential benefit of control devices.[15,16] Several numerical studies have tried to characterise the three-dimensional buffet on a complete wing. Some authors have simulated the shock unsteadiness using ZDES and have argued that a URANS approach is not suited to reproduce the complex phenomenon of three-dimensional buffet.[17] A similar conclusion was drawn from the first Aeroelastic Prediction Workshop,[18] where RANS simulations were shown to be insufficient for the correct physical modelling of the shock-induced vibration on a flexible wing. However, promising results have presented the capability of URANS to simulate transonic tail buffet on a wing-body-tail model for a wide range of angles of attack,[19] reproduced the shock motions on simple three-dimensional configurations,[20] or described the transonic buffet phenomenon on a half wing-body configuration at different flow conditions.[21,22] At the same time, high-fidelity approaches are becoming more and more popular in the aeronautical field and have successfully been applied to other configurations. In particular, DDES has been able to reproduce some

*Honorary Fellow, School of Engineering; fulvio.sartor@liverpool.ac.uk
†Lecturer, School of Engineering; sebastian.timme@liverpool.ac.uk

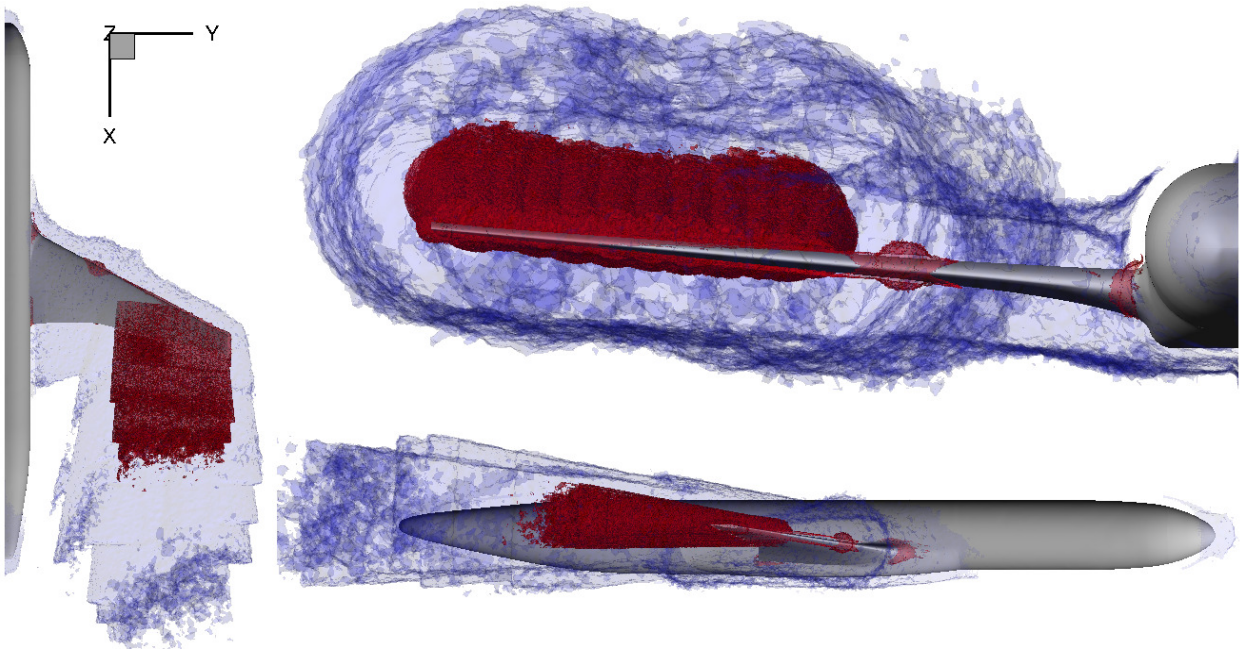

Figure 1. Overview of geometry and refined grid regions obtained with mesh adaptation tool. Blue region shows iso volumes of 10^{-7} m^3; red region shows iso volumes of 10^{-9} m^3.

rather complex flow physics such as separation behind a deflected spoiler on a civil aircraft,[23] the tail buffet phenomenon,[24,25] or the massively separated flow over delta wings[26,27] and complete fighter aircraft.[28]

In this paper we will consider both the URANS and DDES approaches to analyse the flow around a half wing-body configuration at transonic speed. In particular, we focus on the buffet unsteadiness at a given Mach number and fixed angle of attack. The flow conditions relate to wind tunnel tests on the same configuration. In Section II we introduce the numerical approach and the configuration considered. Special attention is given in Section III to the mesh generation for the high-fidelity simulation, which has been carried out using an automated mesh adaptation tool. Section IV then presents the main results discussing steady-state and time-accurate simulations with both URANS and the hybrid method. The unsteady features of the flow are analysed in detail and compared with previous numerical and experimental studies.

II. Numerical Approach

A. Test Case

The chosen test case is a half wing-body configuration, shown in figure 1, representative of a large civil aircraft. The span of the model is 1.10 m, while the aerodynamic mean chord is about 0.279 m. The local chord lengths corresponding to the centre line and wing tip are 0.592 m and 0.099 m, respectively. The wing is twisted, tapered and has a constant sweep angle of 25 deg. This configuration has recently been investigated in the transonic wind tunnel facility of the Aircraft Research Association in the United Kingdom.

The simulations are set up to reproduce the aerodynamic field of the related wind tunnel tests, details of which are not further discussed in this work. The angle of attack is equal to 3.8 deg and has been chosen following a numerical study based on URANS simulation to assess the onset of the buffet instability.[21] The Mach number is 0.8 while the Reynolds number (based on the aerodynamic mean chord) is 3.75 million. The reference temperature and pressure are 266.5 K and 66 kPa, respectively. Laminar to turbulent transition is imposed on the lower surface at about 5% of local chord, while on the upper surface this is at about 10% outboard of the crank and at 15% inboard. Far-field conditions are applied at a distance corresponding to 25 times the half span of the model (around 90 aerodynamic mean chord). Symmetry boundary condition is applied along the centre plane.

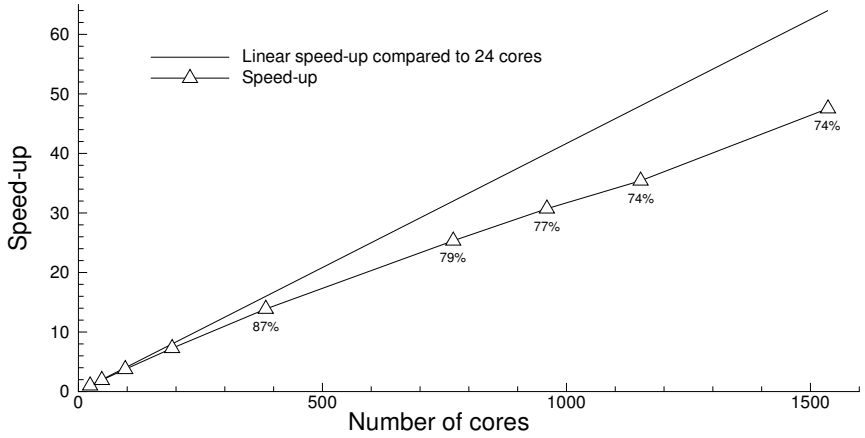

Figure 2. Scaling of DLR-TAU code on ARCHER using adapted mesh with 28.9 M points.

B. Flow Solver

The simulations were performed using the unstructured finite volume solver TAU, developed by the German Aerospace Center (DLR) and widely used in the European aerospace sector. The turbulence model used in the URANS simulation is the negative Spalart-Allmaras (SA) model.[29] Concerning the scale-resolving approach, the flow is investigated using DDES[30] with the original SA turbulence model.[31] Delayed DES is an improved version of the original formulation[32] in terms of preventing the switching to large-eddy simulation (LES) inside boundary layers. A more complete review of this family of scale-resolving simulations, their weaknesses and application can be found in [33].

In the URANS simulation, the second-order central scheme with scalar dissipation was used for the convective fluxes of the Navier-Stokes equations, while a first-order Roe scheme was employed for those of the turbulence model. For DDES, a low dissipative, second-order central scheme with matrix dissipation was chosen for the convective fluxes of the Navier-Stokes and turbulence equations. Gradients of the flow variables, used for the diffusive and source terms, are reconstructed using the Green-Gauss theorem.

While fine-tuning the solver settings for DDES and URANS, it quickly became clear that an optimal setting for DDES is not necessarily suited for the URANS approach. Indeed such URANS simulations gave rather low-amplitude signals for both lift and drag coefficients, and even no buffet at all when using the second-order central scheme for the convective fluxes of the turbulence model. For DDES on the other hand, once a low dissipative setup for the fluxes of the Navier-Stokes equations was established, the choice of the turbulence model discretisation became a minor factor.

Time-accurate computations employ the standard second-order dual-time stepping approach. A dynamic Cauchy convergence criterion is applied for iterations in dual-time. Each time step is iterated until the drag coefficient, chosen as control variable, shows a relative error smaller than 10^{-8} in the last 20 inner iterations. A minimum of 80 and 100 inner iterations is always performed for URANS and DDES, respectively, regardless of the drag convergence, while a maximum of 500 inner iterations is imposed when the convergence criterion is not reached before.

C. Resources and Performance

All simulations were run on ARCHER[a], which at the time of writing was the United Kingdom's primary academic research supercomputer. It is a facility built around a Cray XC30 supercomputer providing the central computational resource. For optimal performance the Zoltan library[34] was linked to DLR-TAU to guarantee a proper partitioning of the adapted mesh. To perform scaling tests, the mesh was split into a large number of domains for numbers of cores ranging from 24 to 1536. As shown in figure 2, the DLR-TAU code performs reasonably well in the considered range giving a scalability of over 70% compared to 24 cores. The production job was then run on 960 cores, where the speed-up is around 80%.

[a]Advanced Research Computing High End Resource.

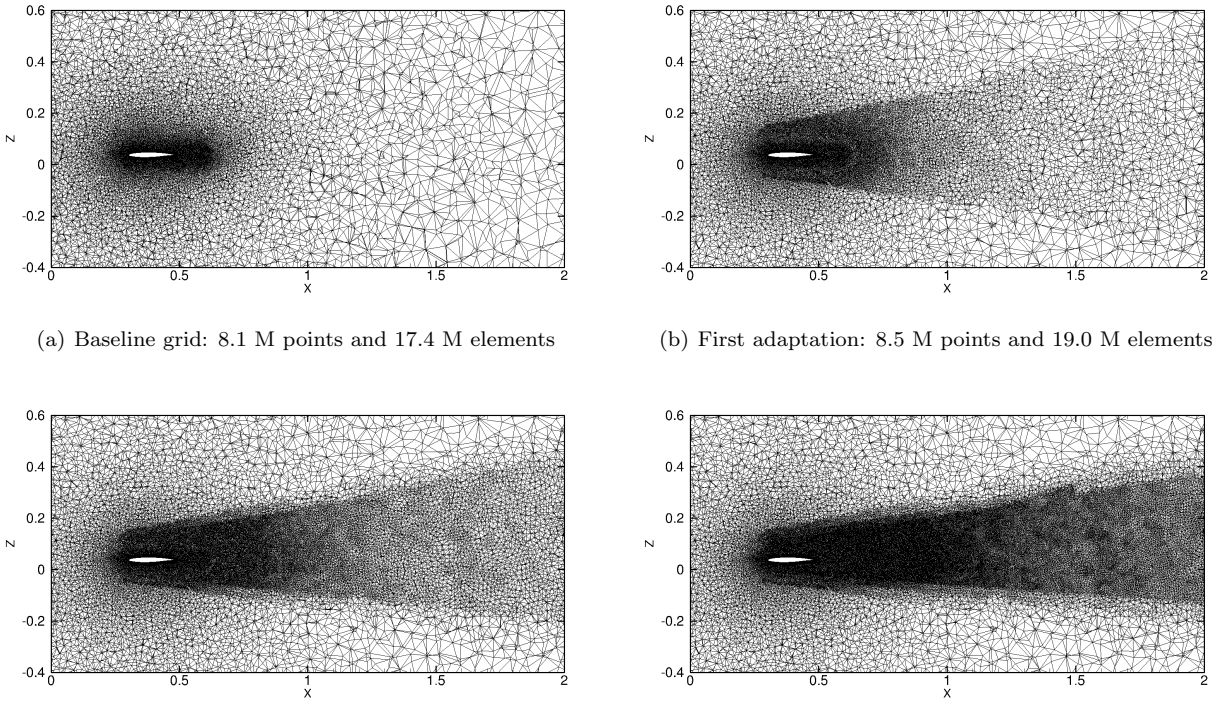

(a) Baseline grid: 8.1 M points and 17.4 M elements

(b) First adaptation: 8.5 M points and 19.0 M elements

(c) Second adaptation: 9.5 M points and 24.9 M elements

(d) Third adaptation: 12.7 M points and 43.5 M elements

Figure 3. Refinement of grid following adaptation and smoothing; slice at 73% span. The fourth adaptation step gives the final mesh with 28.9 M points and 117.1 M elements.

III. Grid Adaptation

For scale-resolving simulations, a highly refined mesh is needed in order to resolve the small turbulent structures present in the separated zone. For the current case, the massively separated flow represents only a small portion of the flow field, so that a uniform refinement of the computational domain is not an efficient approach. The Chimera technique was initially considered but then quickly discarded due to the rather poor performance of the DLR-TAU code. The flow solver performs grid interpolation of the Chimera block at each physical time step even though the connectivity is not changing, thus slowing down the overall simulation.

Another important grid technology is adaptive mesh refinement, where the mesh is refined locally in a given zone of the domain based on some specified criterion. This approach seems to be particularly well suited for DDES and has successfully been applied before.[26] The main requirements of a local refinement strategy are the detection of grid areas to be refined and the method of element subdivisions resulting from insertion of new points in the identified areas. The adaptation tool of DLR-TAU uses an edge based approach. This means that the refinement indicators are evaluated for all edges, new points are inserted at mid-points of selected edges and the element subdivisions are determined from the layout of refined edges. The refinement tool also includes surface approximation and reconstruction for curved surfaces when adding new surface points, and modification of the first cell height (not used though to keep the normal wall-spacing constant). Details of the numerical implementation of the grid refinement can be found in [35, 36].

Due to the time-varying location of the massively separated zone in a buffet investigation, a large portion of the wing has been selected for refinement following a preliminary URANS simulation, which was run for several buffet periods at the same flow conditions using the baseline grid. This non-refined grid has previously been created using the Solar grid generator[37] and thoroughly analysed.[21] The refinement region was then selected in order to cover high values of the time-averaged eddy viscosity. Based on this information, twelve frustums, as indicated in figure 1, are defined spanning the outer wing sections and wake. A representation of the refined zones is visible in the figure as well with the blue surfaces representing cell volumes equal to 10^{-7} m^3, while the red surfaces surround cells with volumes equal to 10^{-9} m^3.

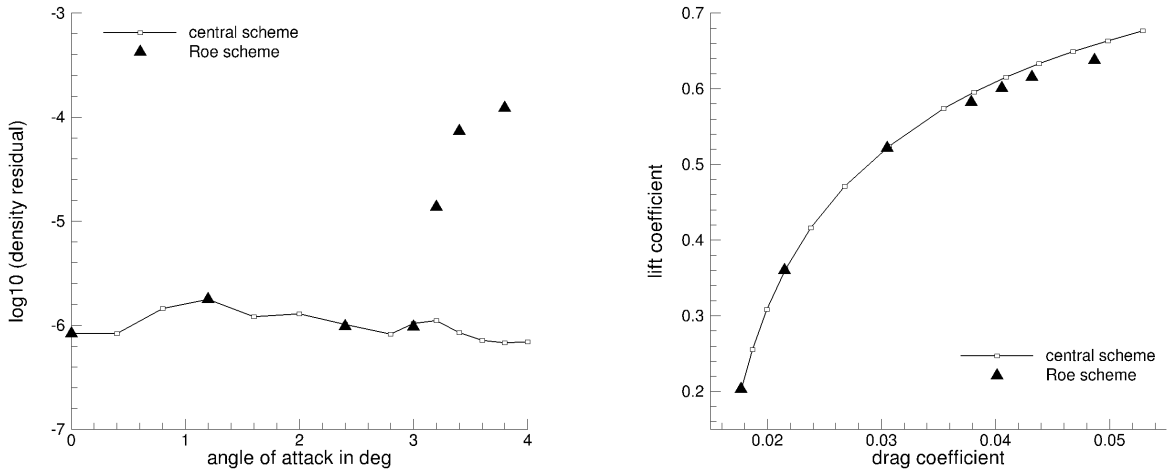

(a) Convergence of density residual

(b) Drag polars

Figure 4. Convergence of density residual and drag polars comparing first-order Roe and second-order central convective schemes for SA turbulence model.

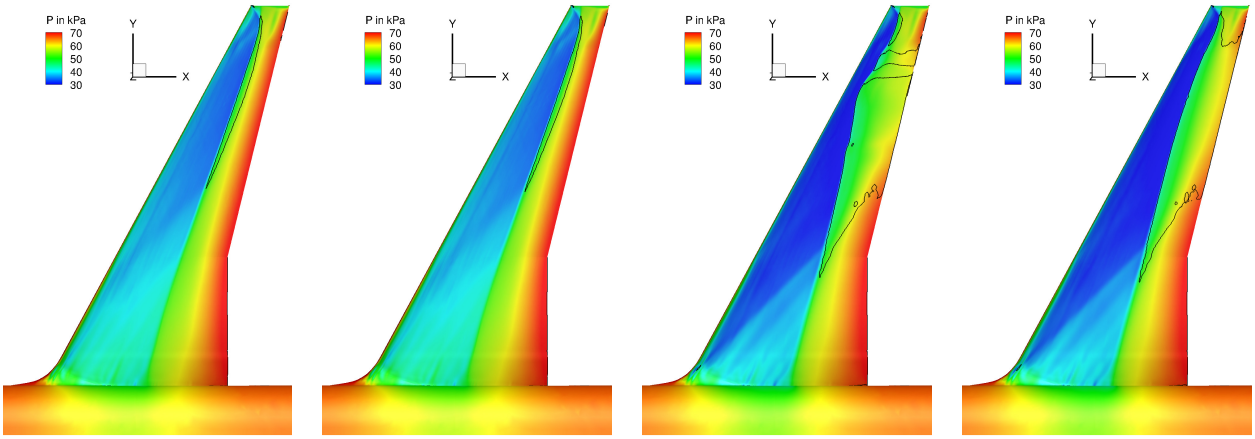

(a) 1^{st} order Roe scheme. 2.4 deg angle of attack

(b) 2^{nd} order central scheme. 2.4 deg angle of attack

(c) 1^{st} order Roe scheme. 3.8 deg angle of attack

(d) 2^{nd} order central scheme. 3.8 deg angle of attack

Figure 5. Surface-pressure distribution and separation line following steady state simulation.

Four steps are needed to obtain the refined grid starting from the baseline version. During each adaptation iteration, only those cells with edges larger than a given value are refined. This value decreases while iterating the adaptation in order to have a gradual refinement. Hexahedral cells in the boundary layer over the wing are also refined in this process to avoid discontinuities in grid spacing towards the surrounding tetrahedral zone. Note that the first three steps are mostly done to obtain a fairly smooth zone in the wake region, while the last step, which is the most expensive to compute, will create the final resolved zone. Grid-smoothing is applied after each adaptation step to obtain a more homogeneous overall spacing. A slice of the domain showing the grid-spacing modification after the first three steps is given in figure 3. The result after the last adaptation step is not included in the figure due to its fineness. The final grid, which is then used for both URANS and DDES investigations, is composed of 28.9 M points and 117.1 M elements. The complete adaptation process can be run in a few hours on a modern workstation.

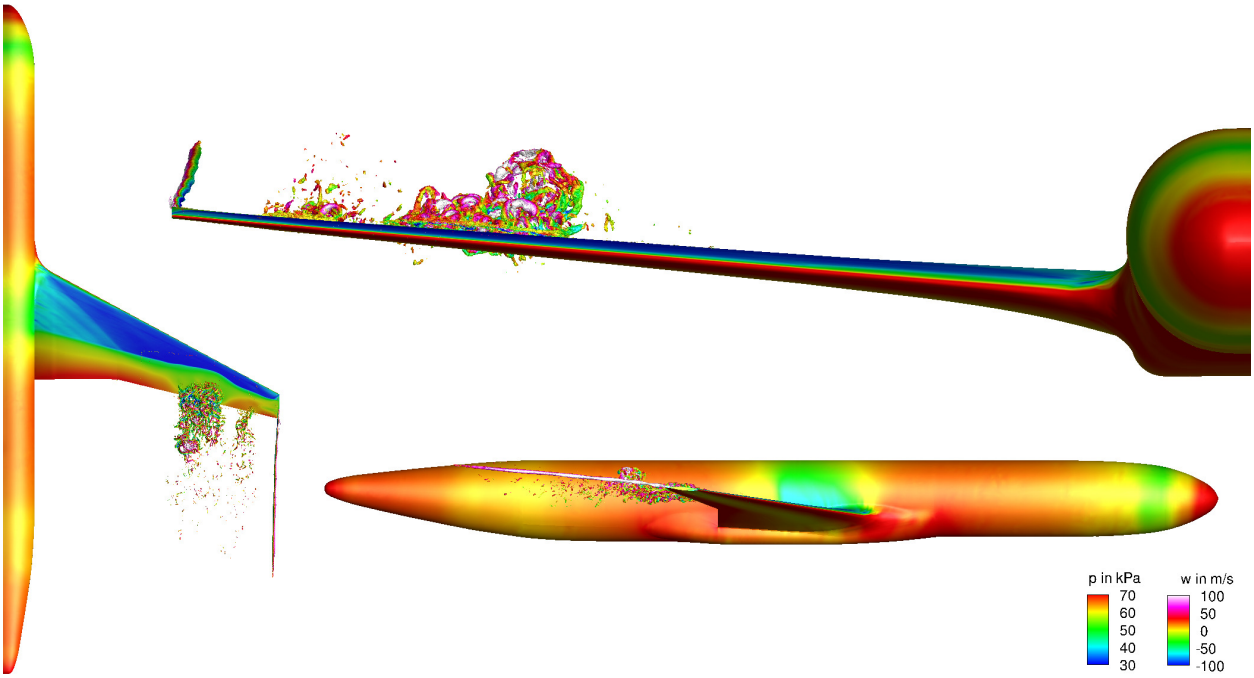

Figure 6. Overview of DDES showing iso contours of Q-criterion at dimensionless value 100.

IV. Results

A. Steady-State Simulations

Reynolds-averaged Navier-Stokes simulations are first performed to converge the governing equations and the results are presented in figures 4 and 5. Simulations at several angles of attack are considered using a first-order Roe and a second-order central scheme for the convective terms of the turbulence model. In figure 4a the evolution of the final density residual normalised by the initial value is plotted over the angle of attack. Focussing on the results obtained with the Roe scheme, when the incidence is smaller than 3.0 deg, the results present a good level of convergence. After this threshold, the final residual rises and the simulation fails to converge to the specified limit. In the case of the central scheme however, the RANS simulations converge towards a steady state regardless, suggesting a failure of the simulation to predict the presence of massively separated flow. The same problem with the central scheme is also encountered when considering time-accurate RANS simulations, but not when using DDES. Figure 4b presents the corresponding drag polar for the steady-state solutions obtained with the two numerical schemes. The agreement is perfect for small angles of attack, while discrepancies are observed once strong shock-wave/boundary-layer interaction is present eventually leading to the shock buffet unsteadiness.

The same behaviour is also found in figure 5, showing the pressure distribution on the surface of the wing. The solid black lines indicate the location of the separated zone by a change in sign of the skin friction coefficient. When considering smaller angles of attack, the solutions are very similar as can be seen in figures 5a and 5b, whereas for higher angles the separated zones differ significantly. The results using the Roe scheme seem to be more reliable since unsteady simulations confirm that the flow field is indeed unsteady. In this case the separated zone is split and the shock foot lays on a curved line, as observed in a previous study.[21] It should be kept in mind however, since the solution presents massively separated zones for high angles of attack, time-accurate simulations should be considered instead to investigate the presence of unsteady flow features.

B. Time-Accurate Simulations

The RANS simulations at 3.8 deg angle of attack are used as starting point for the time-accurate simulations. Once a (partially) converged flow field is obtained, the time discretisation is switched to dual-time stepping

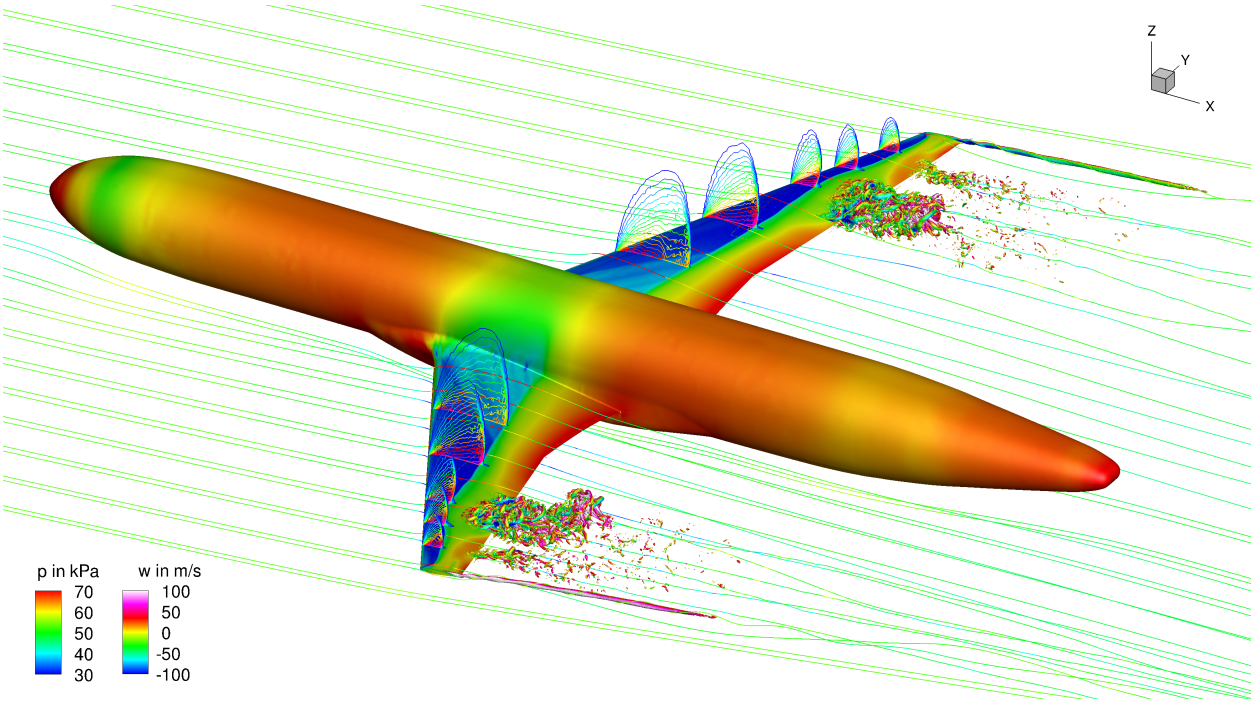

Figure 7. Perspective of DDES showing iso contours of Q-criterion at dimensionless value 100.

with the physical time-step size set to 1 μs. Considering the ratio between a characteristic length (i.e. the aerodynamic mean chord) and a characteristic (i.e. reference) velocity, a convective time typical for the simulation can be defined. In this case the convective time is around 10^{-3} s which is significantly higher than the chosen physical time-step size. The total physical time simulated is 0.1 s, corresponding to about 20 to 30 buffet cycles. A transient part can be observed when the flow develops the unsteadiness. Once this transient has passed, time histories of force and moment coefficients are recorded, and then power spectral density of these signals are analysed for the frequency content of the unsteadiness. Mean and variance of all flow variables are calculated as well; a functionality readily available in the DLR-TAU code.

Figures 6 and 7 show instantaneous iso contours of the Q-criterion at a dimensionless value 100 from different perspectives. The iso contours are coloured by the vertical velocity component, while the wing-fuselage geometry is coloured by the surface pressure distribution. In addition, streamlines coloured by velocity magnitude and contour lines of Mach number are presented in figure 7. The Mach number contours at five span-wise stations indicate the extent of the supersonic region on the suction side of the wing.

Turbulent structures are shed away from the shock foot, which has moved upstream due to the presence of the separated zone. Two separated zones are visible on the wing, each of them responsible for the turbulent structures represented by the Q-criterion. It can be observed that the shock-induced separation, besides causing the presence of the turbulent structures, is responsible for the pressure drop at the trailing edge. The pressure drop causes a decrease in the lift coefficient while increasing the drag. During a buffet cycle, the separated zone moves from the inboard to the outboard portion of the wing, causing periodic variation of forces and moments on the wing. The wing-tip vortex is also visible in the figures through the Q-criterion. Its downstream extent coincides with the highly-refined grid region, as shown in figure 1.

Time histories of the lift and drag coefficients are presented in figure 8. The plot compares the two simulations on the adapted grid with the result obtained in [21] using the baseline non-adapted grid at the same flow conditions. Focussing on the two URANS simulations, it can be seen that the presence of the grid refinement has an impact on the evolution of the forces. However, the average values, the amplitudes of the fluctuations, and the frequency content of the shock motions remain very similar. Looking at the time histories of the forces obtained using DDES, some differences can be noticed. The forces predicted by the URANS approach are higher, which is particularly visible for the lift coefficient presented in figure 8a. Nevertheless, especially when comparing the drag coefficient as shown in figure 8b, the agreement is satisfying. From both figures it is also clear that the high-fidelity approach needs a longer transient to develop the fully established regime, and a longer overall simulation must be considered.

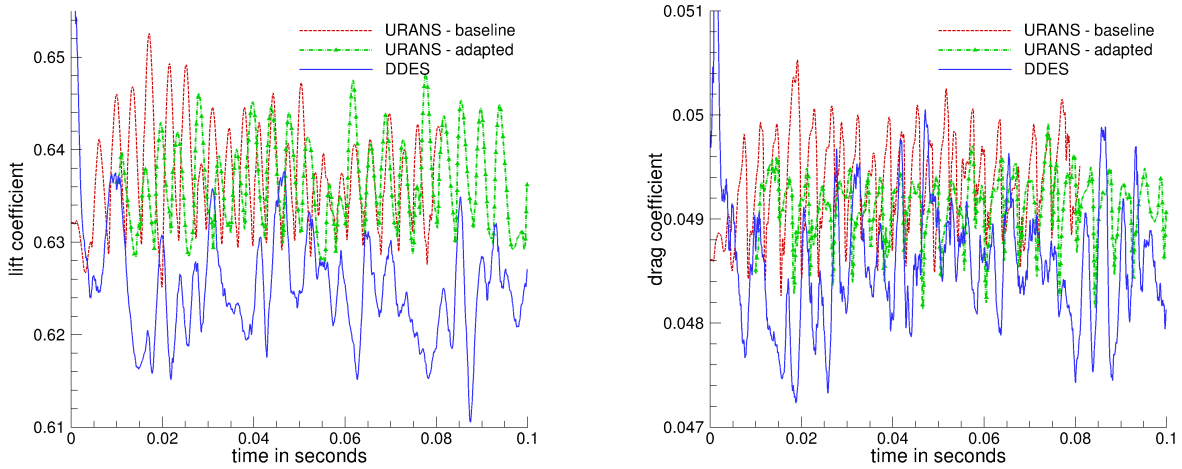

(a) Lift coefficient

(b) Drag coefficient

Figure 8. Time histories of lift and drag coefficients obtained from different simulations.

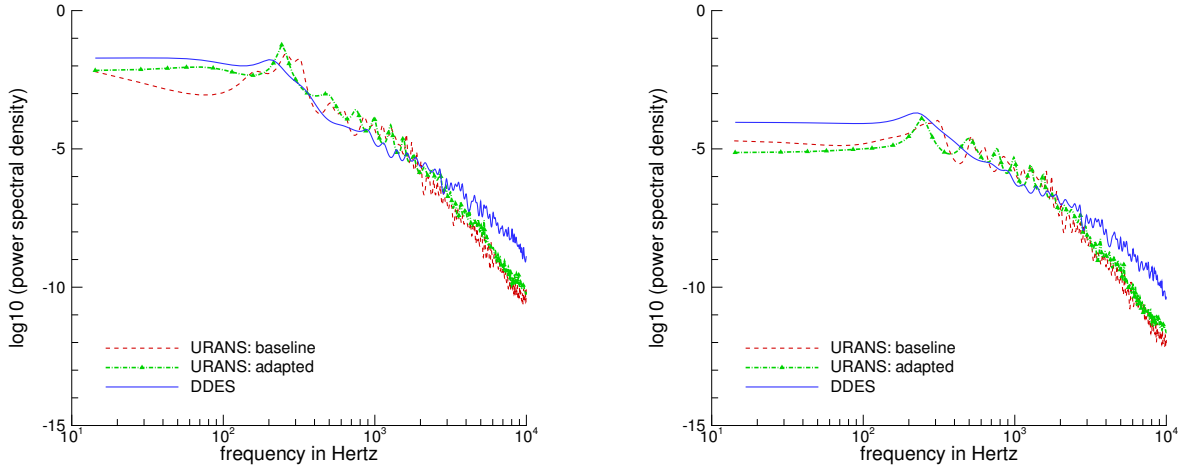

(a) Lift coefficient

(b) Drag coefficient

Figure 9. Power spectral density of lift and drag coefficients obtained from different simulations.

Both simulation approaches can predict transonic buffet, characterised by non-periodic shock motions. These results are compatible with those obtained, on a different configuration, in [17] by means of ZDES. The signals obtained with a URANS approach are less rich in high-frequency fluctuations, probably due to the lack of resolved turbulent content.

Table 1 gives an overview of the average values and standard deviations of the lift and drag coefficients obtained with the different simulation approaches. The statistics are based on a signal of 0.07 s, excluding the transient part of the simulation. The overall grid dependency is limited, since the mesh refinement does not seem to impact the URANS results significantly. The relative error of the average values is less than 0.2% for both lift and drag coefficients. The DDES approach predicts smaller quantities for both lift and drag coefficient, roughly 2% smaller than the URANS approach. Looking at the standard deviations, similar values can be found in all cases.

The frequency content of the shock motions is now discussed by analysing the power spectral density (PSD) of the lift and drag coefficient fluctuations. As pointed out in [38], numerical signals issued from CFD

Table 1. Mean and standard deviation of lift and drag coefficients.

	mean lift	SD lift	mean drag	SD drag
URANS baseline	0.6376	5.328E-03	0.0494	4.300E-04
URANS adapted	0.6367	4.942E-03	0.0491	3.027E-04
DDES	0.6249	5.010E-03	0.0486	5.069E-04

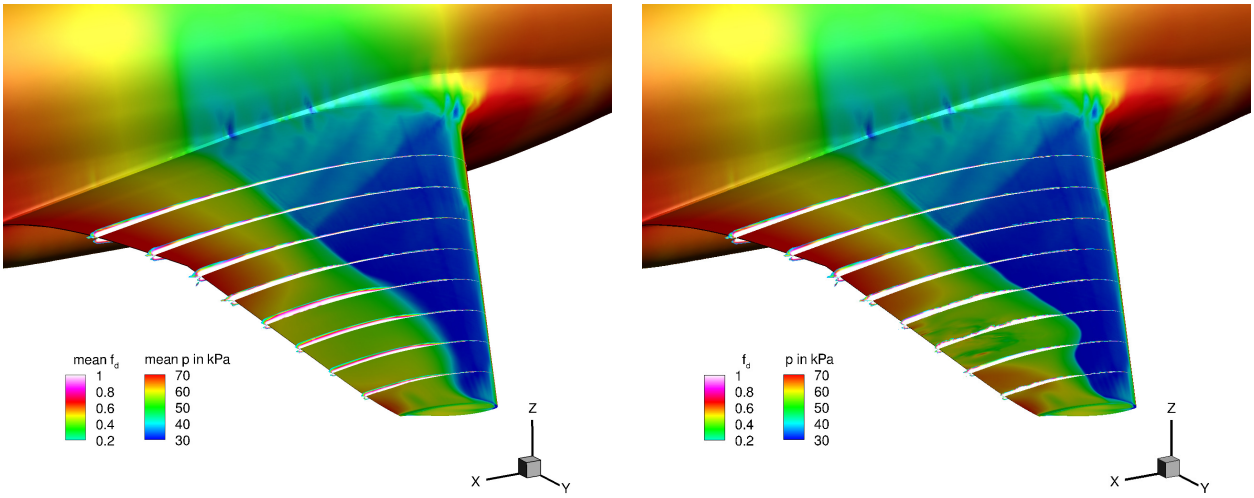

(a) Mean values

(b) Instantaneous at time 0.1 s

Figure 10. Instantaneous and mean surface pressure with slices of delay switch function f_d showing $(1 - f_d)$.

are often oversampled and have a short duration. This can cause a problem since the spectrum definition is linked to the signal length. The solution adopted to overcome this problem is to use an autoregressive estimator,[39] rather than a traditional Fast Fourier Transform. In particular, following the steps outlined in [11], the autoregressive PSD is computed using Burg's (or maximum entropy) method.[40] Each case is analysed using a single window covering the total duration of the signals, without the initial transient. The order of the autoregressive model has been set to 5000 after a parametric study, and is the same for all considered cases.

The results of the PSD thus obtained are presented in figure 9. As for figure 8, the plot includes for comparison also the results obtained using the baseline grid. Very similar conclusions can be drawn analysing either the lift or drag coefficient in figures 9a and 9b, respectively. For all cases, a low-frequency peak can be observed. The peak is broadband, indicating that the shock unsteadiness is characterised by non-periodic motions. Good agreement can be found between the URANS simulations on the baseline and the adapted grid, reconfirming the low impact of the grid refinement on the flow physics. Comparing the PSD of the DDES signals to URANS, the main peak occurs at a slightly lower frequency, indicating that the high-fidelity approach predicts buffet with a longer period. All signals analysed agree on the shock motions occurring at a broadband frequency range between 150 and 300 Hz. This corresponds, once scaled using the non-dimensional time given by the ratio of aerodynamic mean chord and reference velocity, to a Strouhal number of about 0.15 to 0.3. Here again the spectrum is fairly similar to the results obtained in [17] by means of ZDES, without any significant peak in the high-frequency content.

Figure 10 presents instantaneous and mean values of surface pressures and slices of the delay switch function of the DDES formulation called f_d. The plot is showing $(1 - f_d)$ with values close to one indicating RANS mode, whereas values close to zero indicate LES mode. Focussing on the inboard part of the wing, the mean values, presented in figure 10a, equal the instantaneous values, presented in figure 10b. In this region the shielding always gives RANS mode because neither the mesh nor the physics allow it differently. Focussing outboard of the crank, instantaneous changes are clearly visible. In this region the refined part of the mesh is located, and turbulent structures are resolved where significant separation occurs. During grid

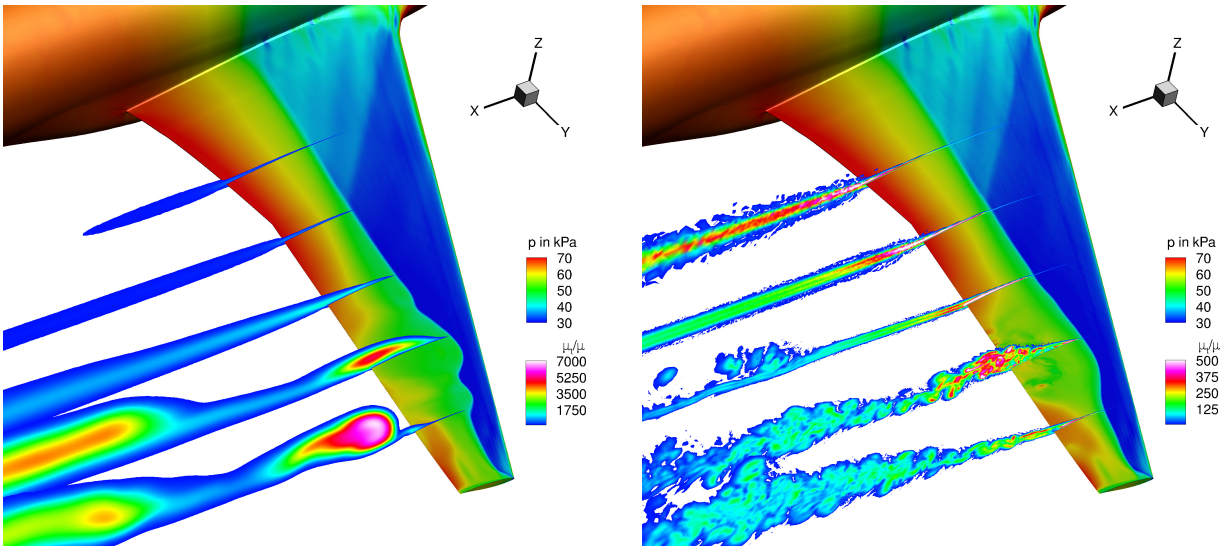

(a) URANS (b) DDES

Figure 11. Instantaneous values of eddy-viscosity ratio.

adaptation, about 21 M points were added in the outboard region of the wing where separation is found. The percentage of grid points which are treated in LES mode has been monitored and the value is always about 70%. This number slightly varies in time, since during the buffet cycle intermittent boundary layer separation and re-attachment occurs. For instance, when the shock is in its most downstream position, no separation can be found in the refined region. Even if the grid spacing allows an LES treatment, the delay switch is not active.

A consequence of the LES treatment in the separated region can be seen from the instantaneous eddy-viscosity ratio, shown in figure 11. The ratio of turbulent (i.e. eddy) viscosity to laminar viscosity is presented. Considering the URANS simulation in figure 11a, the turbulence content is modelled in the entire domain. Very high values of eddy viscosity are clearly visible in the wake of the separated region. More specifically, a blob of eddy viscosity is always present in the wake of the wing region where separation occurs. Since this region varies in time and moves along the wing span periodically, regions with high values of eddy viscosity can also be seen periodically downstream of the wing. Considering an equivalent plot for DDES in figure 11b on the other hand, the simulated part of turbulence is predominant, while the modelled part only causes small values of eddy-viscosity. (Note the scale changes between the two plots.) However, the turbulence content is still modelled in the inboard part of the wing, where the grid spacing does not allow to resolve the detached eddies downstream of the trailing edge. This should not have an influence on the description of the buffet phenomenon, which concerns only the outer part of the wing.

Figure 12 presents the average spatial distribution of the pressure, evaluated at the surface of the wing. The numerical results obtained with URANS and DDES are also compared with a result of the experimental investigation performed in the transonic wind tunnel of the Aircraft Research Association in the United Kingdom using unsteady pressure-sensitive paint. The flow conditions are a Mach number of 0.80 and 4.6 deg angle of attack. The higher experimental angle of attack yields a lift coefficient of 0.625, which is closest to the case considered in the numerical investigation. Note that the computations presented in this work have been performed considering a rigid model, without taking into account the static deformation of the wing in the wind tunnel. Part of the disagreement between the experimental data and the numerical results is due to this approximation.

Comparing DDES and URANS results, excellent agreement can be observed in terms of shock position inboard of the crank. Then, upstream of the separated zone outboard of the crank, a small difference is present. In figure 12a the mean shock foot trace predicted by the URANS approach is more bent in comparison. The DDES results in figure 12b are in better agreement with the experimental investigation. However, comparing the pressure drop at the trailing edge due to the separated zone, the URANS results are in closer agreement with the experiments, while DDES predicts a pressure drop covering a wider part

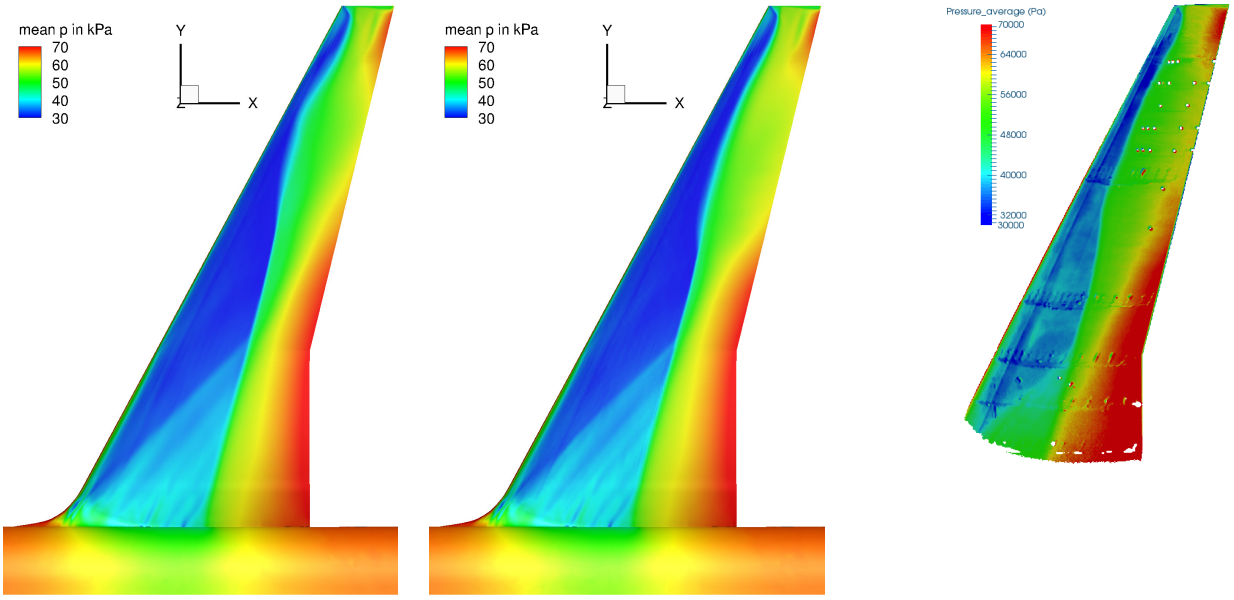

(a) URANS (b) DDES (c) Experimental data

Figure 12. Mean surface-pressure distributions.

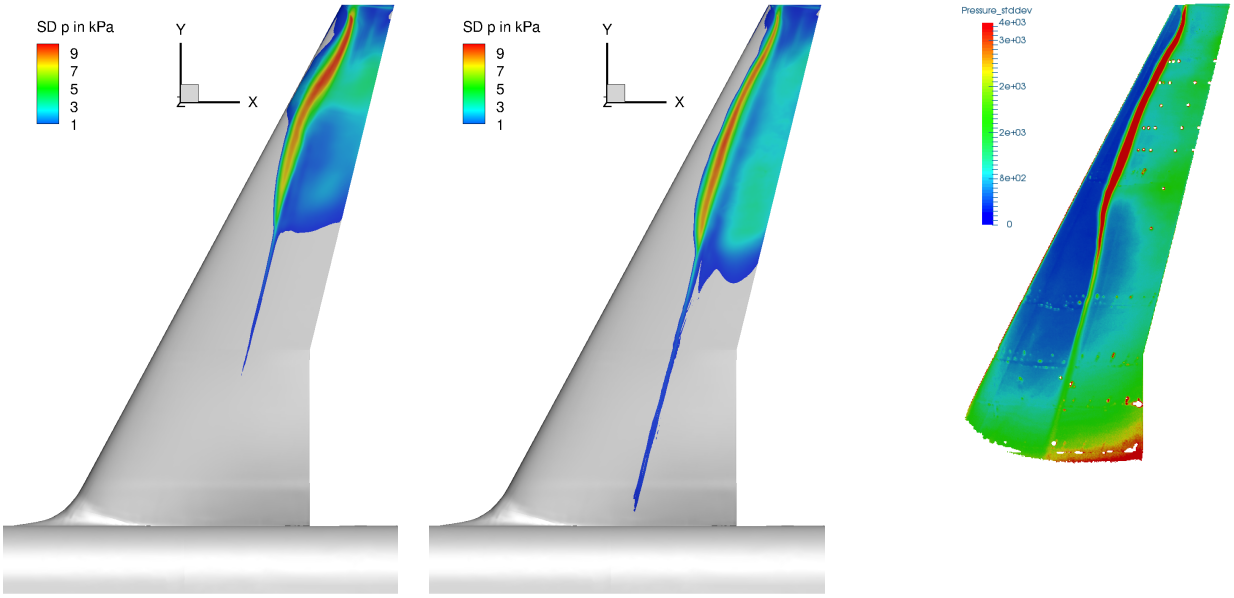

(a) URANS (b) DDES (c) Experimental data

Figure 13. Standard deviation (SD) of surface-pressure distribution.

of the span. This is consistent with the observation of the average values of lift coefficient, as summarised in table 1, giving a slightly lower DDES value than found in the URANS simulations. Finally, it is worth mentioning that the results of the preliminary RANS simulations obtained with a first-order Roe scheme, presented in figure 5c, compare favourably with these figures.

During the unsteady simulations the standard deviation of the fluctuating pressure is computed as well, giving access to the spatial distribution of the unsteady part of the flow. Figure 13 presents the pressure standard deviation, evaluated at the surface of the wing. As for the previous figure, the numerical predictions are compared to experimental results obtained with unsteady pressure-sensitive paint. In all cases the shock foot is characterised by high values of pressure fluctuation, especially upstream of the separated region.

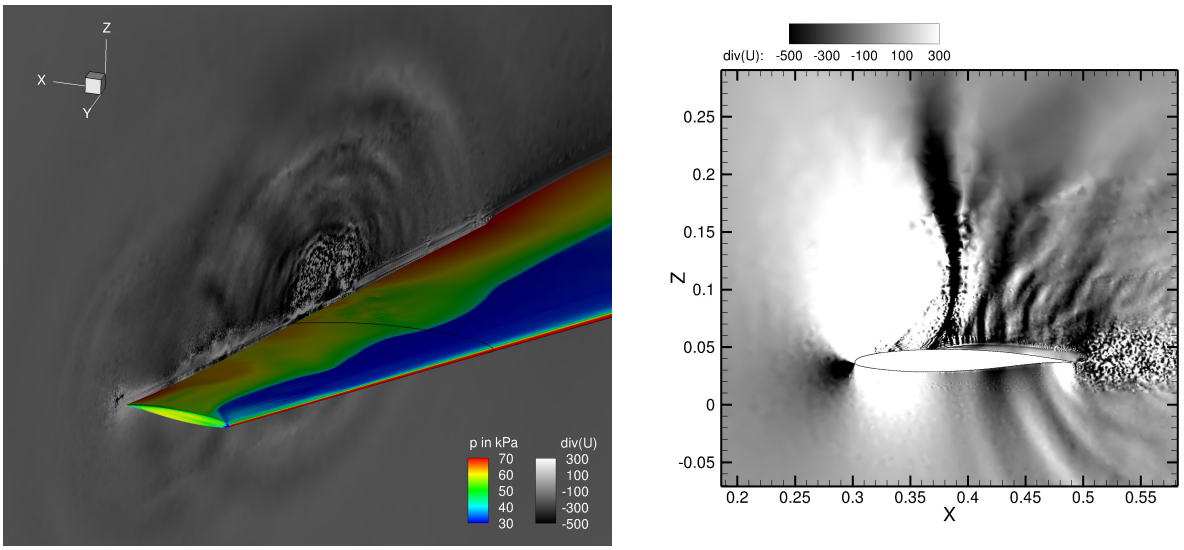

(a) Slice parallel to outer wing trailing edge

(b) Slice at 73% span

Figure 14. Instantaneous divergence of velocity field at time 0.092 s showing pressure waves generated by the separated zone.

However, the unsteadiness is also inboard of the crank. Figures 13a and 13b indicate that the entire shock foot is unsteady, regardless the presence of downstream separation. The bulk of the unsteadiness lays on a bent line for both numerical and experimental results. A very similar shock-foot trace has been observed in previous studies on a wing with a different planform[17] and on a infinite-swept configuration.[20] The main consequence is that the distance between the shock foot and the trailing edge is not constant along the wing span. This feature has been linked to the buffet frequency in a previous work.[21]

Only for the URANS simulation, presented in figure 13a, high pressure fluctuations are visible even near the leading edge, especially close to the wing tip. This feature is neither present in the DDES results nor the experimental data in figures 13b and 13c. However, a leading edge without pressure fluctuations has been observed in URANS simulations when considering different angles of attack[21] or Mach numbers.[22] Concerning the experimental result of figure 13c, the unsteady shock pattern appears to be much closer to DDES than URANS simulations. Also, the unsteadiness in the separated region downstream of the shock foot agrees closer to DDES. The slightly increased levels of pressure variance near the wing-root trailing edge is an systematic experimental error due to variations in intensity reflected by the pressure-sensitive paint.

The interaction between large-scale turbulent structures and the trailing edge causes acoustic radiation. Figure 14 shows an instantaneous divergence of the velocity field to illustrate such pressure waves as previously observed by means of ZDES in [11] in the flow around a supercritical aerofoil. In particular, figure 14a presents a slice downstream and parallel to the trailing edge on the outer part of the wing highlighting the presence of pressure waves generated by the separated zone and propagating away from the source. Upstream travelling disturbances originating at the trailing edge are visible in the slice at 73% span shown in figure 14b. Note that the solid black line included on the surface of the wing in figure 14a describes the location of the slice at 73% span.

As pointed out in [17] for another half wing-body configuration, the propagation process is a three-dimensional phenomenon. This can be seen in figure 14 from both the stream-wise and span-wise propagating waves affecting the dynamics of the shock motion and separation line. The propagating waves can thus generate a feedback mechanism, as proposed in [41] for the two-dimensional case, which must be then be extended to the three-dimensional situation. In a recent paper it was argued that the reason for the broadband-frequency nature of three-dimensional buffet (rather than distinct periodic shock motions) has to be sought in the three-dimensionality of the shock pattern.[21] Unlike the two-dimensional case, the stream-wise distance travelled by the acoustic waves before hitting the shock is not constant along the span of a three-dimensional wing. Thus, the buffet phenomenon is not characterised by perfectly periodic motions. These conclusions will be investigated further.

V. Conclusions

The aim of the present work is to analyse the flow over a large civil aircraft at cruise conditions. At a fixed Mach number the angle of attack is increased until a massively separated region appears on the suction side of the wing. Unsteady flow, known as transonic buffet, is observed. A standard URANS simulation is first conducted on a baseline grid, and it is shown to be capable of reproducing the typical shock motions. Mesh adaptation is then considered to refine the grid in the region of the computational domain relevant to the unsteadiness. Using the highly refined grid, both URANS and DDES approaches are investigated to predict the shock buffet phenomenon. Results of the simulations are presented with particular focus on those of the high-fidelity hybrid approach.

Concerning the shock unsteadiness, the lift fluctuations show that, unlike the two-dimensional case, the unsteadiness is not limited to a periodic oscillation. The unsteady separated zone extends from the wing tip to the crank, and shock motions influence the flow over the entire wing. The frequency content of the lift fluctuations indicates that shock motions occur at frequencies between 150 and 300 Hz. The results agree with conclusions drawn from previous experimental and numerical shock buffet investigations.

In general, the shock unsteadiness appears at time scales which are much longer than those of the wall-bounded turbulence. Thus, a numerical simulation solving the RANS equations in a time-accurate manner closed with a turbulence model is justified. Such unsteady RANS simulations are capable to predict, within the limits of a RANS approach, the main features of the flow. However, the results obtained from DDES provide a more thorough description of the flow physics involved in the buffet phenomenon. A qualitative comparison between simulation results and experimental data indicates closer agreement for the scale-resolved simulation.

Acknowledgements

The authors are grateful to Simon Lawson from Aircraft Research Association for the inspection of the wind tunnel model and for providing the experimental data. The authors wish also to acknowledge Marco Hahn from the same organisation for generating the baseline meshes. The research leading to these results has received funding from the European Union's Seventh Framework Programme (FP7/2007-2013) for the Clean Sky Joint Technology Initiative under grant agreement n°336948. This work used the ARCHER UK National Supercomputing Service (`http://www.archer.ac.uk`).

References

[1]Lee, B. H. K., "Self-sustained shock oscillations on airfoils at transonic speeds," *Progress in Aerospace Sciences*, Vol. 37, No. 2, 2001, pp. 147–196.

[2]McDevitt, J. B., Levy, J. L. L., and Deiwert, G. S., "Transonic flow about a thick circular-arc airfoil," *AIAA Journal*, Vol. 14, No. 5, 1976, pp. 606–613.

[3]McDevitt, J. B. and Okuno, A. F., "Static and dynamic pressure measurements on a NACA 0012 airfoil in the Ames high Reynolds number facility," *NASA TP-2485*, 1985.

[4]Jacquin, L., Molton, P., Deck, S., Maury, B., and Soulevant, D., "Experimental study of shock oscillation over a transonic supercritical profile," *AIAA Journal*, Vol. 47, No. 9, 2009, pp. 1985–1994.

[5]Barakos, G. and Drikakis, D., "Numerical simulation of transonic buffet flows using various turbulence closures," *International Journal of Heat and Fluid Flow*, Vol. 21, No. 5, 2000, pp. 620–626.

[6]Goncalves, E. and Houdeville, R., "Turbulence model and numerical scheme assessment for buffet computations," *International Journal for Numerical Methods in Fluids*, Vol. 46, No. 11, 2004, pp. 1127–1152.

[7]Thiery, M. and Coustols, E., "Numerical prediction of shock induced oscillations over a 2D airfoil: Influence of turbulence modelling and test section walls," *International Journal of Heat and Fluid Flow*, Vol. 27, No. 4, 2006, pp. 661–670.

[8]Crouch, J. D., Garbaruk, A., Magidov, D., and Travin, A., "Origin of transonic buffet on aerofoils," *Journal of Fluid Mechanics*, Vol. 628, 2009, pp. 357–369.

[9]Sartor, F., Mettot, C., and Sipp, D., "Stability, receptivity and sensitivity analyses of buffeting transonic flow over a profile," *AIAA Journal*, Vol. 53, No. 7, 2015, pp. 1980–1993.

[10]Iorio, M. C., González, L. M., and Ferrer, E., "Direct and adjoint global stability analysis of turbulent transonic flows over a NACA0012 profile," *International Journal for Numerical Methods in Fluids*, Vol. 76, No. 3, 2014, pp. 147–168.

[11]Deck, S., "Numerical simulation of transonic buffet over the OAT15A airfoil," *AIAA Journal*, Vol. 43, No. 7, 2005, pp. 1556–1566.

[12]Grossi, F., Braza, M., and Hoarau, Y., "Prediction of Transonic Buffet by Delayed Detached-Eddy Simulation," *AIAA Journal*, 2014, pp. 1–13.

[13]Huang, J., Xiao, Z., Liu, J., and Fu, S., "Simulation of shock wave buffet and its suppression on an OAT15A supercritical airfoil by IDDES," *Science China Physics, Mechanics and Astronomy*, Vol. 55, No. 2, 2012, pp. 260–271.

[14]Mérienne, M.-C., Sant, Y. L., Lebrun, F., Deleglise, B., and Sonnet, D., "Transonic buffeting investigation using unsteady pressure-sensitive-paint in a large wind tunnel," *AIAA Paper 2013–1136*, 2013.

[15]Dandois, J., Molton, P., Lepage, A., Geeraert, A., Brunet, V., Dor, J.-B., and Coustols, E., "Buffet Characterisation and Control for Turbulent Wings," *Aerospace Lab*, Vol. 6, 2013.

[16]Sugioka, Y., Numata, D., Asai, K., Koike, S., Nakakita, K., and Koga, S., "Unsteady PSP Measurement of Transonic Buffet on a Wing," *AIAA Paper 2015–0025*, 2015.

[17]Brunet, V. and Deck, S., "Zonal-detached eddy simulation of transonic buffet on a civil aircraft type configuration," *AIAA Paper 2008–4152*, 2008.

[18]Dalenbring, M., Jirasek, A., Heeg, J., and Chwalowski, P., "Initial Investigation of the Benchmark SuperCritical Wing Configuration using Hybrid RANS-LES modeling," *AIAA Paper 2013–1799*, 2013.

[19]Illi, S. A., Fingskes, C., Lutz, T., and Krämer, E., "Transonic Tail Buffet Simulations for the Common Research Model," *AIAA Paper 2013–2510*, 2013.

[20]Iovnovich, M. and Raveh, D. E., "Numerical Study of Shock Buffet on Three-Dimensional Wings," *AIAA Journal*, Vol. 53, No. 2, 2015, pp. 449–463.

[21]Sartor, F. and Timme, S., "Reynolds-Averaged Navier-Stokes Simulations of Shock Buffet on Half Wing-Body Configuration," *AIAA Paper 2015-1939*, 2015.

[22]Sartor, F. and Timme, S., "Mach number effects on buffeting flow on a half wing-body configuration," *50th 3AF International Conference on Applied Aerodynamics. Toulouse, France*, 2015.

[23]Gand, F., "Zonal detached eddy simulation of a civil aircraft with a deflected spoiler," *AIAA Journal*, Vol. 51, No. 3, 2012, pp. 697–706.

[24]Morton, S., Cummings, R. M., and Kholodar, D. B., "High resolution turbulence treatment of F/A-18 tail buffet," *Journal of Aircraft*, Vol. 44, No. 6, 2007, pp. 1769–1775.

[25]Illi, S. A., , Lutz, T., and Krämer, E., "Transonic Tail Buffet Simulations on the ATRA Research Aircraft," *Computational Flight Testing*, Springer, 2013, pp. 273–287.

[26]Mitchell, A. M., Morton, S. A., Forsythe, J. R., and Cummings, R. M., "Analysis of delta-wing vortical substructures using detached-eddy simulation," *AIAA Journal*, Vol. 44, No. 5, 2006, pp. 964–972.

[27]Morton, S., "Detached-eddy simulations of vortex breakdown over a 70-degree delta wing," *Journal of Aircraft*, Vol. 46, No. 3, 2009, pp. 746–755.

[28]Morton, S. A., Forsythe, J. R., Squires, K. D., and Cummings, R. M., "Detached-eddy simulations of full aircraft experiencing massively separated flows," *The 5th Asian Computational Fluid Dynamics Conference*, 2003.

[29]Allmaras, S. R., Johnson, F. T., and Spalart, P. R., "Modifications and clarifications for the implementation of the Spalart-Allmaras turbulence model," *ICCFD7-1902, 7th International Conference on Computational Fluid Dynamics, Big Island, Hawaii*, 2012.

[30]Spalart, P. R., Deck, S., Shur, M. L., Squires, K. D., .Strelets, M. K., and Travin, A., "A new version of detached-eddy simulation, resistant to ambiguous grid densities," *Theoretical and computational fluid dynamics*, Vol. 20, No. 3, 2006, pp. 181–195.

[31]Spalart, P. R. and Allmaras, S. R., "A one–equation turbulence model for aerodynamic flows," *AIAA Paper 92–0439*, 1992.

[32]Spalart, P. R., Jou, W. H., Strelets, M., and Allmaras, S. R., "Comments on the feasibility of LES for wings, and on a hybrid RANS/LES approach," *Advances in DNS/LES*, Vol. 1, 1997, pp. 4–8.

[33]Spalart, P. R., "Detached-eddy simulation," *Annual Review of Fluid Mechanics*, Vol. 41, 2009, pp. 181–202.

[34]Boman, E. G., Catalyurek, U. V., Chevalier, C., and Devine, K. D., "The Zoltan and Isorropia Parallel Toolkits for Combinatorial Scientific Computing: Partitioning, Ordering, and Coloring," *Scientific Programming*, Vol. 20, No. 2, 2012, pp. 129–150.

[35]Alrutz, T. and Orlt, M., "Parallel dynamic grid refinement for industrial applications," *ECCOMAS CFD 2006: Proceedings of the European Conference on Computational Fluid Dynamics, Egmond aan Zee, The Netherlands, September 5-8, 2006*, Delft University of Technology; European Community on Computational Methods in Applied Sciences (ECCOMAS), 2006.

[36]Alrutz, T. and Vollmer, D., "Recent Developments of TAU Adaptation Capability," *MEGADESIGN and MegaOpt-German Initiatives for Aerodynamic Simulation and Optimization in Aircraft Design*, Springer, 2009, pp. 3–19.

[37]Martineau, D. G., Stokes, S., Munday, S. J., Jackson, A. P., Gribben, B. J., and Verhoeven, N., "Anisotropic hybrid mesh generation for industrial RANS applications," *AIAA Paper 2006-534*, 2006.

[38]Deck, S. and Nguyen, A. T., "Unsteady side loads in a thrust-optimized contour nozzle at hysteresis regime," *AIAA Journal*, Vol. 42, No. 9, 2004, pp. 1878–1888.

[39]Kay, S. M. and Marple, S. L. J., "Spectrum analysis – a modern perspective," *Proceedings of the IEEE*, Vol. 69, No. 11, 1981, pp. 1380–1419.

[40]Burg, J. P., "Maximum entropy spectral analysis," *Modern Spectrum Analysis*, Edited by D. G. Childers, IEEE Press, New York, 1978, pp. 34–41.

[41]Lee, B. H. K., "Oscillatory shock motion caused by transonic shock boundary-layer interaction," *AIAA Journal*, Vol. 28, No. 5, 1990, pp. 942–944.